Improving the numerical performance of transmission line models in EMTP

J. L. Naredo, Jean Mahseredjian, J. A. Gutierrez-Robles, Octavio Ramos-Leaños,
Christian Dufour, Jean Belánger

Abstract-- **This paper deals with the numerical efficiency improvement of transmission line models being applied to power system transient simulation. Although the WB model (or ULM) is more general than FD–Line (or J Marti), the combined use of both is recommended here. Main reasons are that FD–Line offers good numerical performance and applies to very common cases of lines. Use of Vector Fitting with FD–Line is also proposed here to attain low–order rational fits. Techniques are also provided to handle efficiently the complex states being introduced by Vector Fitting in both models, FD–Line and WB. Two of the techniques provided at least double the numerical efficiency of these models.**

Keywords: **Electromagnetic transients, EMTP, real–time, accelerated–time, transmission lines and cables, line models, JMarti model, FD–line, WB model, ULM.**

I. INTRODUCTION

THE design and operation of modern power systems relies each time more on extensive electromagnetic transient (EMT) studies. As these systems grow in size and complexity, the time required for their study becomes excessive. An important research goal is thus to improve the computational efficiency of EMT simulations. Transmission line and cable models are essential components of EMTP programs [1] and this paper focuses on improving the numerical efficiency of two of the principal line models in EMTP; namely, the FD-Line or J. Marti model [2,3], and the Wide–Band (WB) or Universal Line Model (ULM) [4]. Although the WB model is more general than FD–Line, it is considered here that both models should be used in combination. The main reasons for continuing using FD–Line are its high numerical efficiency, its applicability to a large class of lines found in practice and its robustness proven by nearly three decades of use.

The standard FD-Line model in EMTP uses a rational

J. L. Naredo is with Cinvestav Guadalajara, Mexico, (Corresponding author e–mail: jlnaredo@gdl.cinvestav.mx).
Jean Mahseredjian is with Ecole Polytechnique de Montreal, Canada, (e–mail: jean.mahseredjian@polymtl.ca)
J. A. Gutierrez-Robles is with Department of Mathematics, University of Guadalajara, Guadalajara, Mexico, (e-mail: alberto.gutierrez@cucei.udg.mx).
Octavio Ramos-Leaños is with Ecole Polytechnique de Montreal, Canada, (e–mail: octavio.ramos@polymtl.ca)
Christian Dufour is with Opal RT Technologies, Inc., Canada, (e–mail: Christian.dufour@opal-rt.com)
Jean Belánger is with Opal RT Technologies, Inc., Canada, (e–mail: jean.belanger@opal-rt.com)

fitting process based on Bode asymptotic analysis [3,5], whereas the WB model employs the Vector Fitting utility (VF) [6,7]. The Bode–based fitter creates rational fits with real poles, only. VF can provide fits of similar accuracy with a much lower number of poles (*i.e.*, lower order); however, some of these poles can become complex. Other proposition of this paper is to use VF for both models, FD–Line and WB, since their numerical performance is directly related to their rational fit orders.

One issue requiring special consideration regarding the use of VF is the handling of the complex state variables produced by the complex poles. The standard approach a direct one consisting in treating all internal states as complex. In the case of the real states, the imaginary parts simply are zeros. In the case of complex states, the imaginary parts must cancel each others as complex poles and states arise in conjugate pairs. Clearly, for the purposes of this paper this standard approach is highly inefficient. The alternative proposed here is to handle all state variables with real Arithmetic. Various methods for doing this are proposed and analyzed in this paper and their tests have been conducted in the eMEGAsim simulator from Opal-RT Technologies, Inc.

II. TRAVELING WAVE LINE MODELS

Electromagnetic waves propagating along multi–conductor lines and cables are described by the following Telegrapher Equations in frequency domain [1]:

$$\frac{dV}{dx} = -ZI \qquad \text{and} \qquad \frac{dI}{dx} = -YV \qquad \text{(1a,b)}$$

where V is an N-dimensional vector formed with the voltages at the N independent conductors of the line, I is the vector containing the corresponding N–conductor independent currents and Z and Y are the respective $N \times N$ matrices of series impedances and of shunt admittances. These two matrices are in per unit length (*p.u.l.*).

According to (1a) and (1b) the following two expressions represent traveling waves of currents propagating along a line:

$$I_{FW}(x) = I(x) + Y_c V(x) \quad \text{and} \qquad \text{(2a)}$$
$$I_{BW}(x) = I(x) - Y_c V(x), \qquad \text{(2b)}$$

where Y_c is the characteristic admittance matrix of the line

$$Y_c = Y^{-1}\Gamma \qquad \text{(2c)}$$

and Γ is the matrix of line propagation coefficients

$$\Gamma = \sqrt{YZ} \ . \qquad \text{(2d)}$$

I_{WF} corresponds to a wave traveling forwards (*i.e.*, in the positive direction of x), while I_{WF} (2b) corresponds to a backwards traveling wave.

Figure 1 depicts a multi–conductor line–segment of length $x=L$. According to traveling wave properties:

$$I_{FW}(x+L) = H\,I_{FW}(x) \tag{3a}$$

and $\quad I_{BW}(x-L) = H\,I_{BW}(x), \tag{3b}$

where H is the propagation (transfer) matrix of the multi–conductor line–segment:

$$H = \exp(-\boldsymbol{\Gamma} L). \tag{3c}$$

On evaluating (3b) at $x=L$ and from end–conditions in Fig. 1:

$$I_0 - Y_c V_0 = -H[I_L + Y_c V_L]. \tag{4a}$$

Evaluation of (3a) at $x=0$ and application of Fig. 1 end–conditions yields:

$$I_L - Y_c V_L = -H[I_0 + Y_c V_0]. \tag{4b}$$

Expressions (4a) and (4b) provide a basis for the FD–Line [2] and the WB [4] line models. Figure 2 illustrates a circuit representation of a multi–conductor line that is based on (4a) and (4b). According to this figure, the line side at $x=0$ is described as follows:

$$I_0 = I_{sh-0} - I_{aux-0}, \tag{5a}$$

where

$$I_{sh-0} = Y_c V_0, \tag{5b}$$

$$I_{aux-0} = H\,I_{tw-L} \tag{5c}$$

and $\quad I_{tw-L} = I_L + Y_c V_L \tag{5d}$

Vector I_{tw-L} at (5c) and (5d) represents the wave departing from $x=L$ and traveling towards $x=0$, and I_{aux-0} is this same wave after being attenuated and delayed as it arrives at $x=0$. The set of equations that describes the line side at $x=L$ can be obtained exchanging sub–indexes "0" and "L" in (5a–d).

III. MODAL ANALYSIS

Let be assumed that the YZ matrix product is similar to a diagonal matrix $\boldsymbol{\Lambda}$ [8]:

$$T^{-1}YZT = \boldsymbol{\Lambda},$$

where its non-zero elements are the eigenvalues of YZ:

$$\boldsymbol{\Lambda} = diag(\lambda_1,\ \lambda_2,\ \dots,\ \lambda_N),$$

T is the matrix whose columns are the eigenvectors of YZ –or modes of currents, while the rows of T^{-1} are the eigenvectors of ZY –or voltage modes [9,10]. Matrix T further defines the following modal transformations:

$$I^m = T^{-1} I \qquad \text{and} \qquad V^m = T^T V, \tag{6a–b}$$

where T^T represents T–transpose. Transformed vectors I^m and V^m are said to be in the modal domain.

Consider now the matrix

$$\boldsymbol{\Gamma}^m = diag(\gamma_1, \gamma_2, \dots, \gamma_N) \tag{7a}$$

whose non–zero elements are related to those of $\boldsymbol{\Lambda}$ as follows

$$\gamma_i = {}^+\!\sqrt{\lambda_i} = \alpha_i + j\beta_i; \quad i = 1,2,\dots,N. \tag{7b}$$

Here the symbol ${}^+\!\sqrt{}$ indicates the complex root whose real part is positive. γ_i corresponds to the propagation coefficient of the i–th mode, either of current or of voltage. The real part of γ_i is the mode attenuation in Nepers $p.u.l.$, while the imaginary part is the phase–shift of the mode in radians $p.u.l.$ Matrices $\boldsymbol{\Gamma}$ and $\boldsymbol{\Gamma}^m$ are related as follows [9,10]:

$$\boldsymbol{\Gamma} = T\,\boldsymbol{\Gamma}^m T^{-1} \tag{8a}$$

Note that the square of (8a) certainly is YZ.

Consider further the following matrix:

$$H^m = \exp(-\boldsymbol{\Gamma}^m L) = diag(H_1^m, H_2^m, \dots, H_N^m) \tag{8b}$$
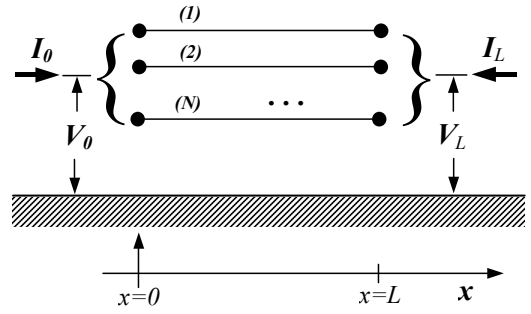

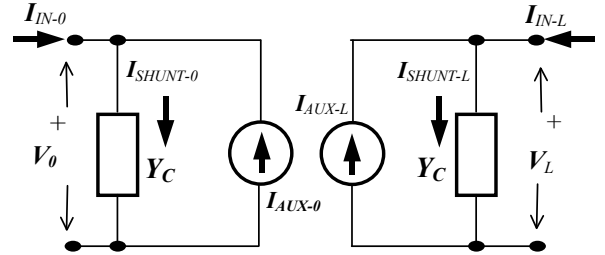Fig. 1. Multi–conductor line segment of length $x=L$.

Fig. 2. Circuit representation of a multi–conductor line derived from traveling wave relations.

with diagonal elements

$$H_i^m = \exp(-\gamma_i \ell); \quad i = 1,2,\dots,N \tag{8c}$$

Matrix H in (3c) can thus be expressed as follows [9,10]:

$$H = T\,H^m T^{-1}, \tag{8d}$$

Hence, H_i^m is the i–th eigenvalue of H corresponding to the propagation transfer function of the i–th mode. Modal characteristic admittance matrix is defined as follows:

$$Y_c^m = T^{-1} Y_c T^{-T}. \tag{9}$$

Whereas the triple matrix products of (8a) and (8d) correspond to similarity transformations, the one in (9) does not; nevertheless, Y_c^m is diagonal [10,11] and its i–th non–zero element is denoted hereafter as $Y_{c,i}^m$.

IV. FD–LINE MODEL

The following description of the FD–Line model differs in several ways from that in [2,3]; nevertheless, the main features of this model are maintained: 1) model is stated in the modal domain, 2) modal transformations are performed through real and constant matrices, 3) frequency dependence is accounted for by means of rational function realizations.

As modal transformations (6a) and (6b) are applied to (5a–d), the following expressions are obtained:

$$I_0 = T I_{sh-0}^m - T I_{aux-0}^m, \tag{10a}$$

$$I_{sh-0}^m = Y_c^m V_0^m, \tag{10b}$$

$$I_{aux-0}^m = H^m I_{tw-L}^m \tag{10c}$$

and $\quad I_{tw-L}^m = I_L^m + Y_c^m V_L^m. \tag{10d}$

A companion set of equations for the line terminal at $x=L$ is obtained interchanging sub–indexes "0" and "L" at (10a–d).

Matrix Y_c^m is diagonal and (10b) is thus equivalent to the following set of N scalar equations that are decoupled:

$$I_{sh-0,i}^m = Y_{c,i}^m V_i^m; \quad i = 1,2,\dots,N. \tag{11a}$$

Since $\boldsymbol{H^m}$ is diagonal as well, (10c) is equivalent to the following set of N decoupled scalar equations:

$$I_{aux-0,i}^m = H_i^m I_{tw-L,i}^m\;; \quad i = 1,2,...,N \qquad (11b)$$

The time domain form of (10a), (11a), (11b) and (10d) is as follows:

$$\boldsymbol{i_0} = \boldsymbol{Ti_{sh-0}^m} - \boldsymbol{Ti_{aux-0}^m}\,, \qquad (12a)$$

$$i_{sh-0,i}^m = y_{c,i}^m \otimes v_{0,i}^m;\quad i = 1,2,...,N\,, \qquad (12b)$$

$$i_{aux-0,i}^m = h_i^m \otimes i_{tw-L,i}^m\;;\quad i = 1,2,...,N \qquad (12c)$$

and $\qquad \boldsymbol{i_{tw-L}^m} = \boldsymbol{i_L^m} + \boldsymbol{y_c^m\,v_L^m}\,, \qquad (12d)$

where lower case variables represent the time domain images of their upper–case counterparts and the symbol $\otimes$ represents the convolution operation.

Expressions (12a–d) fully describe the time domain model of the multi–conductor line–end at $x=0$. The expressions corresponding to the other end at $x=L$ are obtained interchanging sub–indexes "0" and "L" in (12a–d). Expression (12a) basically describes the interface of the line–end model with a general nodal network–solver, which typically is the EMTP. Expression (12d) is made of values being calculated by the model of line–end $x=L$. Thus, the principal tasks of model (12a–d) are the evaluation of the convolutions involved in (12b) and (12c) and this is accomplished effectively by means of State Space analysis [2,3,12].

State Space techniques are introduced as terms $Y_{c,i}^m$ and H_i^m in (11a) and (11b) are represented by rational functions. Rational fitting processes are greatly facilitated when the functions to be fitted are of minimum phase [2,13]. The H_i^m terms in (11b) are not; nevertheless, the following factorization can be first applied [2,3]:

$$H_i^m = H_{min,i}^m \exp(-s\tau_i), \qquad (13a)$$

where $H_{min,i}^m$ is the minimum phase factor, $exp(-s\tau_i)$ is a pure delay term and τ_i is a travel time attributed to the i–th mode velocity. Then, $H_{min,i}^m$ is fitted conveniently as follows:

$$H_{min,i}^m = \sum_{k=1}^{Nh_i} \frac{r_{i,k}}{s - p_{i,k}}, \qquad (13b)$$

where, Nh_i is the order of the fit, $p_{i,k}$ is the k–th fitting pole and $r_{i,k}$ is the corresponding residue.

Let now (13a) and (13b) be introduced in (11b):

$$I_{aux,i}^m = \sum_{k=1}^{Nh_i} X_{i,k}\,, \qquad (14a)$$

where the following Nh_i state variables have been defined:

$$X_{i,k} = \frac{r_{i,k} \times I_{tw-L,i}^m \times \exp(-s\tau_i)}{s - p_{i,k}};\quad k = 1,2,...,Nh_i\,, \qquad (14b)$$

Finally, application of the inverse Laplace Transform to (14b) and subsequently to (14b) results in the following continuous–time state–space (CTSS) forms for calculating the $i_{aux-0,i}^m$ terms of (12c) in time domain.

$$\frac{dx_{i,k}}{dt} = p_{i,k}x_{i,k} + r_{i,k}\, i_{tw-L,i}^m(t - \tau_i);\quad k = 1,2,...,Nh\,, \quad (15a)$$

$$i_{aux-0,i}^m = \sum_{k=1}^{Nh_i} x_{i,k}\,. \qquad (15b)$$

CTSS forms for calculating the $i_{sh0,i}^m$ terms at (12b) are derived by introducing first the following rational approximation for Y_C [3]:

$$Y_{c,i}^m = g_{0,i} + \sum_{k=1}^{Ny_i} \frac{g_{i,k}}{s - q_{i,k}} \qquad (16)$$

where Ny_i is the order of the fit, $q_{i,k}$ is the k–th pole, $g_{i,k}$ is the corresponding residue and $g_{0,i}$ is the following constant term

$$g_{0,i} = \lim_{s\to\infty} Y_{c,i}^m(s).$$

Then, on introducing (16) in (11a) and on applying the inverse Laplace transform the following CTSS form is obtained for evaluating the $i_{sh0,i}^m$ terms at (12b):

$$\frac{dw_{i,k}}{dt} = q_{i,k}w_{i,k} + g_{i,k}v_{0,i}^m;\quad k = 1,2,...,Ny \quad (17a)$$

$$i_{sh-0,i}^m = g_{0,i}v_{0,i}^m + \sum_{k=1}^{Ny_i} w_{i,k} \qquad (17b)$$

Digital simulations require that CTSS forms (15a–b) and (17a–b) be solved numerically. This is done by their conversion to discrete–time state–space (DTSS) which is addressed at sections VI and VII.

One key aspect for the high numerical efficiency of the FD–Line model is the assumption of modal transformations being represented by real and constant matrices. This assumption is correct for loss–less and for perfectly balanced lines. The assumption also is appropriate for nearly balanced aerial lines; that is, for most single or double circuit lines being supported by a single tower structure. Emphasis is made here that these cases of lines are found very frequently in practice.

V. WIDE–BAND LINE MODEL

Modal transformations of highly asymmetric aerial lines, as well as of underground and submarine cables, present considerable variations with frequency and the assumption of constant modal matrices no longer is adequate. The Wide–Band (WB) or Universal Line Model (ULM), first described in [4], accounts for these variations. It does it, however, in an indirect manner.

The basis for the WB model are expressions (5a–d) and a state–space realization of (5b) for calculating $\boldsymbol{I_{sh-0}}$ in time domain can be attained by means of the following rational fitting form of the characteristic admittance matrix $\boldsymbol{Y_C}$ [4]:

$$\boldsymbol{Y_C} = \boldsymbol{G_0} + \sum_{k=1}^{Ny} \frac{1}{s - q_k}\boldsymbol{G_k}\,, \qquad (18)$$

where Ny is the order of the fit, qi is the i–th fitting pole and $\boldsymbol{G_i}$ is the corresponding matrix of residues. $\boldsymbol{G_0}$ is the constant matrix obtained as the limit of $\boldsymbol{Y_C}$ with $s\to\infty$. Note from (18) that common poles are used for the fitting of all elements in Y_C. These poles usually are obtained from the trace of $\boldsymbol{Y_C}$ [13].

The introduction of (18) in (5b), and the subsequent application of the Inverse Laplace Transform results in the following CTSS form for $\boldsymbol{i_{sh-0}}$:

$$\frac{d\boldsymbol{w_k}}{dt} = q_k\boldsymbol{w_k} + \boldsymbol{G_k v_0};\quad k = 1,2,...,Ny \qquad (19a)$$

$$i_{sh-0} = G_0 v_0 + \sum_{k=1}^{Ny} w_k . \qquad (19b)$$

The CTSS form of (5c) for calculating I_{aux-0} is more complicated than that in (19a,b). The major difficulty lays in the effective extracting of multiple line–delays from the H matrix. Early attempts for this consisted in extracting a single delay common to all elements in H [14]. The problem here is that each one of these elements can involve up to N different delays due to multi–mode propagation. Matrix H can be decomposed in the following form that permits complete decoupling and extraction of all delays [15]:

$$H = \sum_{k=1}^{N} Ip_k \times \exp(-\gamma_k \ell), \qquad (20a)$$

where Ip_k denotes the k–th idempotent of H which is the rank 1 matrix obtained by multiplying the k–th column of modal matrix T by the k–th row of its inverse T^{-1} [11]. Each exponential factor in (22a) is further decomposed as follows:

$$\exp(-\gamma_k \ell) = \exp(-\tilde{\gamma}_k \ell)\exp(-s\tau_k), \qquad (20b)$$

where τ_k is a time delay associated to the velocity of the k–th mode and $\tilde{\gamma}_k$ is the k–th modal propagation constant modified accordingly. Hence:

$$H = \sum_{k=1}^{N} \left[Ip_k \times \exp(-\tilde{\gamma}_k \ell)\right] \times \exp(-\tau_k \ell). \quad (20c)$$

At the WB model it is considered that modal delays τ_k usually come in groups of almost identical values. The following decomposition of H is thus put forward [4]:

$$H = \sum_{i=1}^{Ng} \tilde{H}_i \exp(-s\tau_i), \qquad (21)$$

where Ng is the number of delay groups and τ_i is the delay assigned to the i–th group. To decide whether a set of delays form a group, the criterion is that their associated phase shifts should differ in less than a certain angle value, say 10° [4]. Once the group delays have been formed, matrices $\tilde{H}_1, \tilde{H}_2,…, \tilde{H}_{Ng}$ are identified in the phase domain through VF [4]. Comparison between (20c) and (21) yields:

$$\tilde{H}_i = \sum_{k=1}^{I_i} Ip_k \exp(-\tilde{\gamma}_k \ell); \quad k = 1,2,…,Ng , \qquad (22)$$

where I_k is the number of modes belonging to the i–th delay group.

Each element of the $\tilde{H}_i$ matrix in (22) can now be considered a minimum phase function and this whole matrix is approximated effectively as follows [4]:

$$\tilde{H}_i = \sum_{k=1}^{Nh(i)} \frac{1}{s - p_{i,k}} R_{i,k}; \quad i = 1,2,…,Ng \qquad (23)$$

where $Nh(i)$ is the order of the fit, $p_{i,k}$ represents the fitting poles and $R_{i,k}$ the corresponding residue matrices. Note that common poles are used for the fitting of all elements in $\tilde{H}_i$.

On the basis of (5c), (21) and (23), the following state vectors are thus defined:

$$X_{i,k} = \frac{1}{s - p_{i,k}} R_{i,k} I_{tw-L} \exp(-s\tau_i); \quad \begin{array}{l} i = 1,2,…,Ng \\ k = 1,2,…,Nh(i) \end{array} \qquad (24a)$$

and (5c) takes the following form:

$$I_{aux-0} = \sum_{i=1}^{Ng} \sum_{k=1}^{Nh(i)} X_{i,k} . \qquad (24b)$$

Application of the Inverse Laplace Transform in (24a) and

(24b) yields the following CTSS form for i_{aux-0}:

$$\frac{dx_{i,k}}{dt} = p_{i,k} x_{i,k} + R_{i,k} i_{tw-L}(t - \tau_i); \quad \begin{array}{l} i = 1,2,…,Ng \\ k = 1,2,…,Nh(i) \end{array} \qquad (25a)$$

and

$$i_{aux-0} = \sum_{i=1}^{Ng} \sum_{k=1}^{Nh(i)} x_{i,k} . \qquad (25b)$$

CTSS forms (19a,b) and (25a,b) constitute the basis of the WB line model [4]. Solution by a digital processor still requires their conversion to discrete time. Note the similarity of (19a,b) and (25a,b) with (17a,b) and with (15a,b), respectively. The former ones can be regarded as matrix–vector versions of the latter ones.

VI. DISCRETE TIME STATE SPACE FORMS

Conversion from continuous–time to discrete–time state–space (DTSS) forms is described as follows for single–phase lines. Extension to the multi–conductor line case is straightforward. DTSS conversion is attained by applying a numerical differentiation rule to CTSS forms. The mid–point rule of differentiation (or trapezoidal integration) is the preferred one in EMTP. Mid–point rule is equivalent to applying the bilinear transformation to the CTSS forms in Laplace domain [16]:

$$s = \frac{2}{\Delta t} \frac{1 - z^{-1}}{1 + z^{-1}} \qquad (26)$$

where Δt is the simulation time–step and z^{-1} is the one–step Δt delay–operator.

Expression (26) now is applied in (14b), and after an algebraic process and the application of the inverse z–Transform [16], the following relation is obtained:

$$x_k = a_k x'_k + b_k \left[i_{tw-L}(t - \tau) + i'_{tw-L}(t - \tau)\right]; \quad k = 1,2,…,Nh \qquad (27a)$$

where

$$a_k = (2 + \Delta t p_k)/(2 - \Delta t p_k), \qquad (27b)$$

$$b_{i,k} = \Delta t r_{i,k}/(2 - \Delta t p_{i,k}), \qquad (27c)$$

$$x'_k = x_k(t - \Delta t) \qquad (27d)$$

and

$$i'_{tw-L}(t - \tau) = i_{tw-L}(t - \tau - \Delta t). \qquad (27e)$$

Note in this relation that super–index "m" indicating modal domain and sub –index "i" indicating mode number have been dropped. From here on, this change of notation is adopted for the sake of clarity. Expression (14a) becomes then:

$$i_{aux-0} = \sum_{k=1}^{Nh} x_k , \qquad (27f)$$

Note also in (27a), (27d) and (27e) that primed variables denote past values calculated at a previous Δt time–step.

Let be assumed further in (27a–e) that Δt always is smaller than any of the travel–times τ_i of a line being considered. Each x_k variable is then updated by (27a) only from previously calculated values of itself and of i_{tw-L}. For this reason, expressions (27a–e) constitute proper DTSS forms to evaluate the $i_{aux-0,i}^{m}$ terms in the FD–line model and, by a straightforward extension, the $i_{aux-0,k}$ terms in the WB model.

Bilinear transformation (28) is now applied to (11a), along with (16), in the same way as above. The following expression is thus obtained:

$$w_k = a_k w'_k + b_k(v_0 + v'_0), \quad k = 1,2,…,Ny \qquad (28a)$$

The companion expression of (28a) is derived as follows from (17b) by a simple process:

$$i_{sh-0} = g_0 v_0 + \sum_{k=1}^{Ny} w_k , \qquad (28b)$$

One problem with (28a) is that input voltage v_0 appears at the r.h.s. at its present (uncalculated) value, and a proper DTSS form requires that w_k be updated only by past values. This problem is fixed by redefining state variable w_k in a way that it incorporates the undesirable contribution of v_0. The following redefinition is adopted here:

$$(w_k - b_k v_0)/[b_k(a_k + 1)] \rightarrow w_k \qquad (29)$$

On applying (29) in (28a) and (28b):

$$w_i = a_i w'_i + v'_0 ; \quad i = 1,2,\ldots, Ny , \qquad (30a)$$

$$i_{sh-0} = G v_0 + \sum_{k=1}^{Ny} c_k w_k , \qquad (30b)$$

where

$$c_k = b_k(a_k + 1) \quad \text{and} \quad G = g_0 + \sum_{i=1}^{Ny} b_i \qquad (30c,d)$$

Now (30a) and (30b) constitute proper DTSS forms for the sequential evaluation of $i_{sh-0,i}^m$ at the FD–line model and, by their extension to the multi–conductor line case, for the evaluation of $\boldsymbol{i_{sh-0}}$ at the WB model.

VII. Efficient Handling of Complex States

The Bode–based fitter used the with standard FD–Line model in EMTP offers important features, namely: 1) resulting fitting poles are real and stable, and 2) rational approximations are minimum phase. Modal delays τ_i are thus simply determined by direct comparison of the given propagation functions $\tilde{H}_i^m$ with the obtained rational fits. On the other hand, however, rational approximations by the Bode fitter present a much higher order than required. It has been shown in [17], for instance, that a Levenberg–Marquardt algorithm produces approximations of lower order and similar accuracy. Vector Fitting is the standard fitting tool for WB in EMTP and can synthesize rational functions with low order and high accuracy; nevertheless, it can introduce complex poles.

Complex poles are handled at standard WB model of EMTP by declaring all poles and their associate state variables as complex types, even the real ones. By doing this, memory needs are doubled and the number of basic operations is increased, at least twofold for additions and fourfold for multiplications. Complex poles rarely occur in the fitting of $\boldsymbol{Y_c}$ and only between 20% and 40% of the poles related to the fitting of $\boldsymbol{H}$ could be complex. Therefore, the handling of all state variables of a line model as complex types will introduce a large number of trivial operations; i.e., additions of zeros and multiplications by zeros. In addition, since complex states occur in conjugate pairs and both states conveying the same information, the computation of the two of these is redundant.

The proposition in this paper is to adopt VF for both, FD–Line and WB models, and then to handle the resulting complex states by a real Arithmetic process that can be accomplished in various ways. The following ones are analyzed here: 1) first order realizations, 2) second order realizations, 3) fourth order realizations and 5) full order realizations.

A. First order real blocks for complex states.

Assume in (13b) that two of the fitting poles are a complex conjugate pair of the form $p=p_R+jp_I$ and $p^*=p_R -jp_I$, along with their corresponding residues $r=r_R+jr_I$ and $r^*=r_R-jr_I$. The contribution of these two poles to $I_{aux-0,i}^m$ in (14a) is thus:

$$I_X = X_1 + X_2 , \qquad (31a)$$

with

$$X_1 = \frac{r}{s - p} I_{tw-L} \exp(-s\tau) \qquad (31b)$$

and

$$X_2 = \frac{r*}{s - p*} I_{tw-L} \exp(-s\tau). \qquad (31c)$$

Application of the Inverse Laplace Transform in (31a–c) yields the following CTSS form for I_x:

$$i_X = x_1 + x_2 , \qquad (32a)$$

$$\frac{dx_1}{dt} = px_1 + ri_{tw-L}(t-\tau) \qquad (32b)$$

and

$$\frac{dx_2}{dt} = p*x_2 + r*i_{tw-L}(t-\tau). \qquad (32c)$$

Consideration is made now that state variables x_1 and x_2 must be complex conjugates:

$$x_1 = x_R + jx_I \qquad (33a)$$

$$x_2 = x_R - jx_I \qquad (33b)$$

On introducing (36a) and (36b) in (35a) yields:

$$i_X = 2x_R . \qquad (34a)$$

Introduction of (33a,b) in (32b) and the subsequent separation in real and imaginary terms results in the following pair of coupled differential equations:

$$\frac{dx_R}{dt} = p_R x_R - p_I x_I + r_R i_{tw-L}(t-\tau), \qquad (34b)$$

and

$$\frac{dx_I}{dt} = p_R x_I + p_I x_R + r_I i_{tw-L}(t-\tau). \qquad (34c)$$

Further application of (33a,b) in (32c) results again in expressions (34b,c). It is clear, therefore, that (32c) is redundant with (32b). It also is clear that (34a–c) offers a far better alternative than (32a–c), since the former forms are free of redundancies and state variables x_R and x_I are real.

DTSS forms now are obtained applying first the Laplace transform to (34a–c), then the bilinear transform (26) and finally the inverse z–Transform. After an algebraic process:

$$i_X = \xi x_R + \vartheta x_I , \qquad (35a)$$

$$x_R = \phi x'_R - \eta x'_I + e[i_{tw-L}(t-\tau) + i'_{tw-L}(t-\tau)] \qquad (35ab)$$

and $\quad x_I = \phi x'_I + \eta x'_R + f[i_{tw-L}(t-\tau) + i'_{tw-L}(t-\tau)], \quad (35c)$

where coefficients ξ, ϑ, ϕ, η, e and f correspond to expressions (A1–4) in the Appendix. Expressions (35a–c) should be compared with (15a–b).

A similar treatment as the previous one is given next to the complex poles arising at the fitting of Y_C. Assume that there are two complex conjugate poles q and q^* in (16), along with their corresponding residues g and g^*. Let the contribution of these poles to $I_{sh-0,i}^m$ in (11a) be denoted by I_y:

$$I_y = \left(\frac{g}{s - q} + \frac{g*}{s - q*} \right) V_0 \qquad (36)$$

with $g=g_R+jg_I$ and $q=q_R+jq_I$. The following discrete–time

relations are derived from (36) by applying a process analogous to the previous one in (31a–c)

$$i_y = \xi w_R + \vartheta w_I + \rho v_0 , \qquad (37a)$$

$$w_R = \phi w'_R - \eta w'_I + \theta v'_0 \qquad (37b)$$

and

$$w_I = \phi w'_I + \eta w x'_R + \psi v'_0 , \qquad (37c)$$

where w_R and w_I are the two real state–variables replacing the conjugate ones that would be obtained directly from (36). The coefficients ξ, ϑ, ρ, ϕ, η, θ and ψ are given by expressions (A5–8) in the appendix.

B. Second order blocks

Complex states are naturally eliminated as two first order blocks corresponding to a pair of conjugate poles are combined in a single second order block. Expressions (31a–c) thus take the following form:

$$\left(s^2 + \beta_1 s + \beta_0\right) I_X = \left(\alpha_1 s + \alpha_0\right) I_{tw-L} \exp(-s\tau), \qquad (38)$$

with α_0, α_1, β_0 and β_1 given by expressions (A9–12) in the appendix. On applying the bilinear transform (26) in (38),followed by application of the inverse z–Transform:

$$i_x = -c_1 i'_x - c_2 i''_x + d_0 i_{tw-L}(t-\tau) + \\ d_1 i'_{tw-L}(t-\tau) + d_2 i''_{tw-L}(t-\tau), \qquad (39)$$

where c_1, c_2, d_0, d_1 and d_2 are given by expressions (A13–16) in the appendix. Note that expression (38) is a second order difference equation, that i_x can play the role of a state variable to be added to i_{aux-0} in (27f) and that now it is necessary to store the two previous history values i'_x and i''_x, as well as the three previous ones $i_{tw-L}(t-\tau)$, $i'_{tw-L}(t-\tau)$ and $i''_{tw-L}(t-\tau)$.

The second order form for (36) is analogous to (38):

$$\left(s^2 + \beta_1 s + \beta_0\right) I_y = \left(\alpha_1 s + \alpha_0\right) V_0 , \qquad (40)$$

only with q, q^*, g and g^* replacing p, p^*, r and r^*, respectively at (A9–12). Application of the bilinear transform (26) and subsequently the inverse z–Transform in (43) yields:

$$i_y = -c_1 i'_y - c_2 i''_y + d_0 v_0 + d_1 v'_0 + d_2 v''_0 , \qquad (41)$$

with the same coefficients as in (39). Finally, (41) is expressed in proper DTSS form as follows:

$$i_y = d_0 v_0 + w \qquad (42a)$$

and

$$w = -c_1 w' - c_2 w'' + h_1 v'_0 + h_2 v''_0 , \qquad (42b)$$

with

$$h_1 = d_1 - c_1 d_0 \qquad (42c)$$

and

$$h_2 = d_2 - c_2 d_0 \qquad (42d)$$

C. Fourth and higher order blocks

Two second order blocks can be grouped together to form a fourth order block; and one could even group a larger number of first order blocks to attain higher orders. By this, the number of computations required by the line model is decreased. Nevertheless, the sensitivity of the model to round–off errors is increased.

For an M–order block to evaluate i_{aux-0} expression (38) is generalized as follows:

$$\left(s^M + \sum_{i=1}^{M-1} \beta_i s^i\right) I_X = \left(\sum_{i=1}^{M-1} \alpha_i s^i\right) I_{FAR} \exp(-s\tau) \quad (43)$$

Application of the bilinear transformation (26) and the inverse z–Transform yields

$$i_X = -\left(\sum_{i=1}^{M} c_i i_X^{(i)}\right) + \sum_{i=0}^{M} d_i i_{FAR}^{(i)}(t-\tau), \qquad (47)$$

which is a generalization of (42). Note that $i_X^{(i)}$ represents the i–th difference of i_X; that is:

$$i_X^{(i)} = i_X(t - i\Delta t).$$

The M–order block for i_Y in the Laplace domain is equal to (43) with I_Y replacing I_X and V_0 replacing $I_{tw-L}\exp(-s\tau)$. After applying the bilinear transform, followed by the application of the inverse z–Transform and by an algebraic process, the M–th order proper form for i_Y is:

$$i_y = d_0 v_{IN} + w \qquad (48a)$$

and

$$w = -\sum_{i=1}^{M}\left(c_i w^i\right) + \sum_{i=1}^{M} h_i v_{IN}^{(i)} , \qquad (48b)$$

with

$$h_i = d_i - c_i d_0; \quad i = 1,2,\ldots,M . \qquad (48c)$$

Note that expressions (48a–c) are generalizations of (45a–c).

D. Test cases

Consider a 150 km long single–phase line formed by a bundle of four ACSR conductors, each one with a diameter of 2.5 cm and the spacing between adjacent sub–conductors being 45 cm. The line runs horizontally at a medium height of 27 m above a ground -plane with a 100 Ωm resistivity. The line is excited at its sending end by a unit–step current–source with 1/600 S shunt admittance. The far end of the line is open ended. Figure 3 shows a diagram of the line connections.

The response of the line at its two ends is calculated by prototypes of the proposed realizations, as well as of the standard one consisting in the treatment of all states as complex. The prototypes have been executed both, in MatLab and eMEGAsim environments. The latter is for subsequent development of real–time line models. Table I provides the numerical performance, or complexity, of the realizations evaluated as the operation count for one Δt–step update of a system with 12 states. Note that the direct approach for
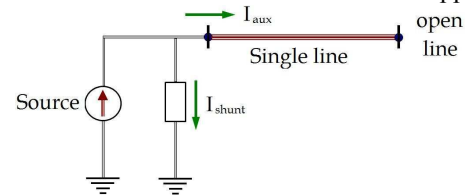

Fig. 3. Test–case, single–phase line connection diagram.

TABLE I
NUMERICAL PERFORMANCE OF REALIZATIONS.

Required Basic Operations for 12 States			
Method	*SUMS*	*MULTS.*	*FLOPS*
1st Ord. pure real	24	24	24
1st Ord. pure complex (Direct implement.)	48	96	96
1st Ord, complex in real Arithmetic	54	54	54
1st Ord, combined, real Arithmetic	30	30	30
2nd Order	25	25	31
4th Order	25	25	29
Full Order	25	25	25

complex states has the poorest performance, while the realizations of first order–combined with real arithmetic and of second order are much more efficient.

Accuracy of the proposed realizations is evaluated comparing their results with those from the Numerical Laplace Transform (NLT) technique as described in [18]. NLT results are produced using *32,172* or more samples, a time–step $\Delta t=1.0$ μs, the Hanning window and a maximum relative error of 10^{-5}. Figure 4 provides the waveform at the sending end as obtained with the NLT, as well as with the abovementioned prototypes. Figure 5 shows a close–up for the two first bends of the sending–end waveform. Note from these figures that the waveforms obtained with first order realizations, as well as with the second order one, are very close to those of the NLT. It can also be noticed there that the waveforms for fourth and full order realizations depart noticeably from those of the NLT and, in addition, in the long run these two waveforms show round–off error accumulation and the eventual frank departure from the theoretically expected response.

Figure 6 provides the voltage waveforms for Fig. 3 circuit at the far end of the line, and Fig. 7 is a close–up for the first three bends of these waveforms. The observations from these figures confirm those of Figs. 4 and 5. The error accumulation effects of the fourth and full order realizations are now more pronounced.

Finally, Fig. 8 provides plots of percent errors for the waveforms at the receiving end by taking the NLT results as the reference.. Important features of these error plots are the overall differences, not the peaks which coincide with reflected wave arrivals, and these peaks are due to slight delay–differences between the reference model (NLT) and the model being evaluated.
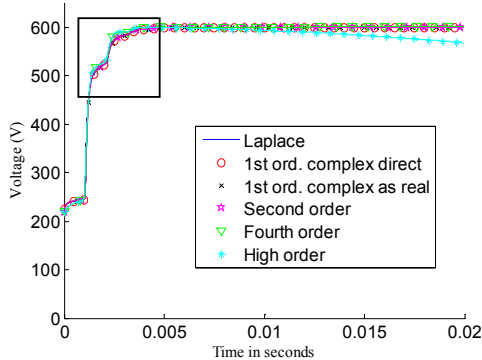

Fig. 4 Sending–end waveforms as obtained with different line models. Inner frame indicates zoom–in area at next figure.
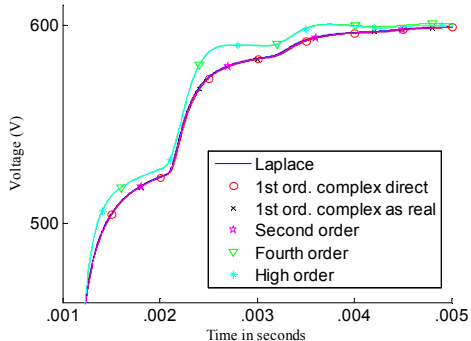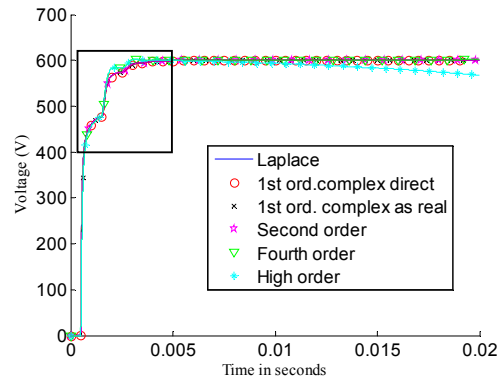

Fig. 5 Close–up of sending–end waveforms.

Fig. 6 Receiving–end waveforms as obtained with different line models. Inner frame indicates zooming–in at the next figure.
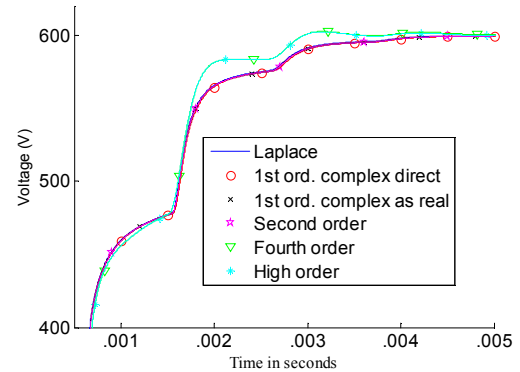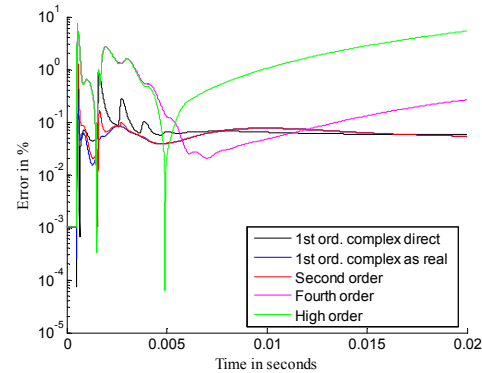

Fig. 7 Close–up of receiving–end waveforms.

Fig. 8 Percent errors for various model realizations at predicting receiving–end waveforms.

VIII. CONCLUSIONS

The research reported in this paper is concerned with the increase of computational efficiency at the transmission line models used in EMT simulations. FD–Line and WB (or ULM) are two of the most relevant models available at the principal versions of EMTP. Although WB is more general, it has been considered here that the use and development of FD–Line should be continued, since it requires less computations than WB and it applies to very common line cases.

First, a unified review of both models, WB and FD–Line, has been presented here. Then, alternatives to improve their computational efficiency have been proposed and analyzed. Application of VF to FD–Line has been recommended to produce low order rational fits while preserving its accuracy.

Rational fits obtained with VF may produce complex states and the standard treatment of these has been ruled out as it results highly inefficient. Instead, it has been proposed here to

handle all internal state variables by processes in real Arithmetic. As conjugate pairs of states carry the same information; it has been shown here that one of these can be discarded, while the other can be handled very efficiently by a pair of equivalent states that are coupled and real.

Other alternatives proposed and analyzed here consist in the realizations of line models by means of second, fourth and higher order blocks of states. Higher order realizations involve less computations; however, as the order of the blocks is increased, the model becomes more sensitive to the round–off errors in the digital representation of the model coefficients.

Several tests have been applied to the proposed alternatives. Their accuracy has been evaluated by means of the Numerical Laplace Transform [18]. Test results have shown that first order realizations with real arithmetic, as well as second order realizations, are the most accurate and do not present round–off error accumulation, even after 200 s of simulated time. Fourth and higher order realizations, on the other hand, do accumulate those errors rather soon. As for numerical performance both realizations, first order ones with real Arithmetic and second order ones, are about three times more efficient than the standard implementations of WB in EMTP.

IX. APPENDIX

Coefficients for expressions (35a–c):

$$\phi = 1 + \frac{4\Delta t p_R + 2(\Delta t p_R)^2 - 4(\Delta t p_I)^2}{4 - 4\Delta t p_R - 3(\Delta t p_R)^2}. \tag{A1}$$

$$\eta = (8\Delta t p_I)/\left[4 - 4\Delta t p_R - 3(\Delta t p_R)^2\right]. \tag{A2}$$

$$e = \left(4\Delta t r_R - 2\Delta t^2 p_R r_R - 4\Delta t^2 p_I r_I\right)/\left[(2 - \Delta t p_R)^2\right]. \tag{A3}$$

$$f = \left(4\Delta t r_I - 2\Delta t^2 p_I r_I + 4\Delta t^2 p_I r_R\right)/(2 - \Delta t p_R)^2. \tag{A4}$$

Coefficients for expressions (37a–c):

$$\phi = 4(2 - \Delta t q_R)/\left[(2 - \Delta t q_R)^2 + (\Delta t q_I)^2\right] - 1 \tag{A5}$$

$$\eta = 4\Delta t q_I/\left[(2 - \Delta t q_R)^2 + (\Delta t q_I)^2\right] \tag{A6}$$

$$\theta = \eta\left[g_R/q_I - (\Delta t g_I)/(2 - \Delta t q_R)\right] \tag{A7}$$

$$\psi = \eta\left[g_I/q_I - (\Delta t g_R)/(2 - \Delta t q_R)\right] \tag{A8}$$

Coefficients for expression (38):

$$\alpha_0 = -2[\Re\mathbf{e}\{r\}\times\Re\mathbf{e}\{p\} + \Im\mathbf{m}\{r\}\times\Im\mathbf{m}\{p\}] \tag{A9}$$

$$\alpha_1 = 2\Re\mathbf{e}\{p\} \tag{A10}$$

$$\beta_0 = |p|^2 \tag{A11}$$

$$\beta_1 = -2\Re\mathbf{e}\{p\} \tag{A12}$$

Coefficients for expression (39):

$$c_1 = -(2\beta_0\Delta t^2 - 8)/den \tag{A13}$$

$$c_2 = -(\beta_0\Delta t^2 - 2\beta_1\Delta t + 4)/den \tag{A14}$$

$$d_0 = (\alpha_0\Delta t^2 + 2\alpha_1\Delta t)/den \tag{A15}$$

$$d_1 = 2\alpha_0\Delta t^2/den + c_1 \times d_0 \tag{A16}$$

$$d_2 = (\alpha_0\Delta t^2 - 2\alpha_1\Delta t)/den - c_2 \times d_0 \tag{A17}$$

$$den = \beta_0\Delta t^2 + 2\beta_1\Delta t + 4$$

X. REFERENCES

[1] Dommel, H.W., EMTP Theory Book, Microtran Power System Analysis Corporation, 4689 W. 12th. Avenue, Vancouver, B.C. V6R 2R7, Canada, 2nd. edition, May 1992.

[2] J. R. Marti, "Accurate Modeling of Frequency-Dependent Transmission Lines in Electromagnetic Transient Simulations." IEEE Transactions on Power Apparatus and Systems, Vol. PAS-101, pp. 147-157, 1982.

[3] Jose R. Marti, "The Problem of Frequency Dependence in Transmission Line Modeling", PhD Thesis, Department of Electrical Engineering, The University of British Columbia, April 1981.

[4] Atef Morched, Bjǿrn Gustavsen,, Manoocher. Tartibi, "A universal model for accurate calculation of electromagnetic transients on overhead lines and underground cables", IEEE Trans. on Power Delivery, Vol. 14, No. 3, pp. 1032-1038, July 1999.

[5] Hendrik W. "Bode, Network Analysis and Feedback Amplifier Design", D Van Nostrand Company, Toronto, New York, London, 1945.

[6] Gustavsen, B.; Semlyen, A., "Rational approximation of frequency domain responses by vector fitting," *Power Delivery, IEEE Transactions on* , vol.14, no.3, pp.1052-1061, Jul 1999.

[7] Bjorn Gustavsen, "User's Guide for vectfit3.m", Available at: http://www.energy.sintef.no/Produkt/VECTFIT/index.asp, August 2008.

[8] Naredo, J. Luis, Faria, J. A. Brandao; da Silva, J. F. Borges; , "Discussion of "Wave Propagation in Polyphase Transmission Lines a General Solution to Include Cases Where Ordinary Modal Theory Fails" [Discussion and closure to discussion]," *Power Delivery, IEEE Transactions on* , vol.1, no.2, pp.188-189, April 1986.

[9] Hedman, D. E.; , "Propagation on Overhead Transmission Lines I-Theory of Modal Analysis," *Power Apparatus and Systems, IEEE Transactions on* , vol.84, no.3, pp.200-205, March 1965.

[10] Wedepohl, L.M.; , "Electrical characteristics of polyphase transmission systems with special reference to boundary-value calculations at power-line carrier frequencies," *Electrical Engineers, Proceedings of the Institution of* , vol.112, no.11, pp.2103-2112, November 1965.

[11] L. M. Wedepohl, "Frequency Domain Analysis of Wave Propagation in Multiconductor Transmission Systems", Lecture Notes, Univ. of British Columbia, Dept. of Electrical Engineering, Canada, 1993.

[12] Adam Semlyen and Mansour H. Abdel-Rahman, "A State Variable Approach for the Calculation of Switching Transients on a Power Transmission Line", IEEE Transactions on Circuits and Systems, Vol CAS-29, No. 9, pp. 624- , September 1982.

[13] Bjǿrn Gustavsen, John Nordstrom, "Pole Identification for The Universal Line Model Based on Trace Fitting", IEEE Transactions on Power Delivery, Vol. 23, no. 1, pp. 472–479, Jan. 2008.

[14] H. V. Nguyen, H. W. Dommel, J. R. Marti, "Direct Phase Domain Modelling of Frequency-Dependent Overhead Transmission Line", *Power Delivery, IEEE Trans. on*, vol.12, no.3, pp. 1335-1342, Jul 1997.

[15] F. J. Marcano, J. R. Marti, "Idempotent Line Model: Case Studies", IPST'97, International Conference on Power System Transients, Seattle, June 22-26, 1997.

[16] J. G. Proakis and D. G. Manolakis, *Digital Signal Processing. Principles, Algorithms and Applications*, Prentice-Hall, 4th Ed., 2007.

[17] A. B. Fernandes, W. L. A. Neves, "Frequency Dependent Low Order Approximation of Transmission Line Parameters", Proceedings of the IPST-99, International Conference on Power Systems Transients, Budapest, Hungary, June 20-24, 1999.

[18] J. L. Naredo, J. Mahseredjian, Ilhan Kocar, J. A. Gutiérrez–Robles, J. A. Martinez–Velasco, "Frequency Domain Aspects of Electromagnetic Transient Analysis of Power Systems.", IEEE/PES Tutorial on Electromagnetic Transients in Power Systems. Solution Techniques, Applications, Simulation Tool Development, Editor: J. A. Martínez–Velasco, Chapter 3, pp. 20-36, IEEE Code Nr. in Process, July 2010.